15TH IEA HEAT PUMP CONFERENCE
MAY 26–29, 2026 | HOFBURG
VIENNA 2026
DECARBONISATION THROUGH INNOVATION

Prototyping a novel lab-scaled high temperature heat pump connected to a latent thermal energy storage for usage in thermally integrated Carnot batteries

Titouan Janod[a*], Yacine Brahami[b], Vincent Lemort[a]

[a]University of Liège, Thermodynamics Laboratory, Allée de la Découverte 17, 4000 Liège, Belgium
[b]Tecumseh Europe Sales & Logistics, Engineering Department, 2 av de la Libération, 38290 La Verpillière, France

Abstract

Carnot Batteries integration in industrial processes can allow energy storage for damping renewable energies' intermittent production while increasing energy efficiency and decreasing greenhouse gases emissions. In the meantime, small scale High-Temperature Heat Pumps (HTHPs) are highlighted as promising to decrease usage of fossil fuels in small industrial applications. The SEHRENE (Store Electricity and Heat foR climate Neutral Europe) EU-funded project aims to develop a concept of Thermally Integrated Carnot Batteries (TI-CB) through modelling activities on three use cases and through the construction of a prototype, notably. This prototype will mimic one of the use cases representing the most the SEHRENE TI-CB concept. It will be spatially separated in two distinct test rigs, with the HTHP + Thermal Energy Storage (TES) being built at the University of Liège. The TES will be latent-type, filled with phase change material (erythritol, $T_{melting} = 117°C$). The thermal power and temperature level of the test rig were chosen from components availability and literature review as being 10 kW of heating capacity and 135°C of condensing temperature. The HTHP will comprise an evaporator, a condenser, an internal heat exchanger, an expansion valve and two piston compressors. One of the latter will allow studies on compressor cooling, and the other will be used to run the general HTHP coupled with TES. Their role is distinct and they are not meant to run at the same time. A secondary pressurised water loop will be placed between the HTHP and the TES to address manufacturing constrains. It will include a feature to flash the water to allow TES charging both with liquid or two-phase water. The learning outcomes from that test rig to be built could be useful to both small scale machines and for upscaling, studying the dynamics of the test rig, the control strategies, and the compressor cooling.

Selection and/or peer-review under the responsibility of the organizers of the 15th IEA Heat Pump Conference 2026.

Keywords: High Temperature Heat Pump ; Thermal Energy Storage ; Phase-Change Material ; Piston compressor ; Thermally Integrated Carnot Battery

1. Introduction

Thermally-Integrated Carnot Batteries (TI-CB) in industrial processes gained increasing interest in research due to their potential role in storing intermittent renewable energies while improving energy efficiency and reducing greenhouse gases emissions by using unexploited Industrial Waste Heat (IWH). The main advantages of this technology compared to Li-ion batteries are its low dependency on critical raw materials, its longer storage duration, its scalable potential, and the fact that it is based on already existing technologies [1]. In this frame, the EU-founded SEHRENE project [2] aims to develop digital twins for three use cases of TI-CB and one TRL4 prototype. The general concept of SEHRENE TI-CBs consists in a Rankine-based High-Temperature Heat Pump (HTHP) used to charge a Phase-Change Material (PCM) Thermal Energy Storage (TES) from IWH. This PCM-TES is then discharged through an Organic Rankine Cycle (ORC) to produce electricity. One of the three SEHRENE's use cases studies the implementation of a TI-CB in the Kızıldere-2

* Corresponding author. *E-mail address:* titouan.janod@uliege.be

Geothermal Power Plant (GPP) of Zorlu Enerji. This GPP is one of the largest of Türkiye, having 80 MW_e of capacity through its combined triple flash cycle and binary ORC. The identified IWH from this plant comes from an unexploited reinjection well containing geothermal brine at 105°C.

Regarding the TRL4 prototype of TI-CB that is to be developed in the SEHRENE project, the machine will consist of an HTHP fed with hot water mimicking a IWH source to charge a PCM-based TES. The discharge will then be operated by an ORC. The particularity of this machine is that it will be spatially separated in two test rigs: the charging phase experimentations (HTHP+TES) will be led at the University of Liège, in Belgium, while the discharging phase tests (ORC+TES) will be done at CEA Grenoble, France, by another team of the SEHRENE project. As the only common element between the two machines will be the TES, this element shall feature similar characteristics in both locations, chosen as being its thermal power and its capacity. This will allow the pooling of results from both test benches to be combined on the same ground and comparable.

The role of the test rig to be built will be the miniaturisation of the aforementioned Zorlu Enerji use case of the SEHRENE project. The test rig must in the end have some learning outcomes that will benefit the modelling activities of the SEHRENE project, which notably includes the creation of digital twins for every use case. However, some learning outcomes from the test rig will remain specific to small-scale systems and may not translate directly to larger implementations. These will be discussed further in the last part of this paper.

In the literature, HTHPs and TES are usually put together when building test rigs of CBs [3], [4]. Small scale HTHPs, alone or not, were highlighted as being able to replace fossil fuel boilers in market applications such as food, paper, metal and chemical industries, notably for drying processes purposes or sterilisation [5].

This paper will propose a justification for the different choices made for prototyping the HTHP-TES test bench to be built in the University of Liège, according to the following plan: first, the test rig main design choices are presented. Then, the prototype modelling for components choices is described. Finally, the learning potential outcomes from the test bench are addressed.

2. Main design choices

2.1. SEHRENE TI-CB concept miniaturisation

One of the main goals of the SEHRENE project is to lead modelling activities about three use cases. To ensure strong synergy between modelling and experimentation, the test rigs developed in the experimental campaign of the SEHRENE project should embody a miniaturised version of the TI-CB concept promoted by the latter. The use case representing the most this concept is the one studying the implementation of a TI-CB in the Kızıldere-2 GPP of Zorlu Enerji in Türkiye, which first preliminary designs were presented in [6], [7], [8].

This use case consists of an HTHP fed at the evaporator with IWH coming from unused geothermal brine at 105°C to be reinjected in ground. This HTHP comprises an Internal Heat Exchanger (IHX) for increasing performance and guaranteeing sufficient superheating at the compressor's suction. The condenser of the HTHP is materialised by a PCM-based TES. This TES is also the evaporator of the ORC used for discharging the TI-CB. The ORC comprises a recuperator and the Working Fluid (WF) is condensed via an Air-Cooled Condenser (ACC). A pump circulates and pressurises the WF. As the IWH from the geothermal brine is available 24/7, and as the charge (via the HTHP) and the discharge (via the ORC) of the TI-CB will never be operated at the same time, a preheater using this geothermal brine is placed between the recuperator cold side's exhaust and the TES-evaporator's supply of the ORC. The PCM chosen to fill the TES is sebatic acid, melting at 134.8°C. The WF chosen for this use case is cyclopentane. The use case architecture and T-s diagrams are presented on Figure 1. For an intuitive visualisation, secondary fluids are plotted with the entropy of the corresponding WF state points. Table 1 summarises the main results and parameters coming from its current preliminary design.

Table 1: Main results from the current preliminary design of the Zorlu Enerji use case of the SEHRENE project. Details about modelling methodology, inputs and parameters in [9], [10] and [11].

Parameter/ Result	T_{IWH}	T_{PCM}	ΔT_{lift}^{HTHP}	$\dot{W}_{net}^{HTHP}$	$\dot{Q}_{HTHP}$	COP	Q_{TES}	$\dot{W}_{net}^{ORC}$	η_{ORC}	$\Delta t_{charge}/\Delta t_{discharge}$	WF
Unit	[°C]	[°C]	[K]	[MW]	[MW]	[-]	[MWh]	[MW]	[-]	[h]	[-]
Value	105	134.8	45.4	2.0	12.8	5.85	51	3.8	0.125	4/2	Cyclo-pentane

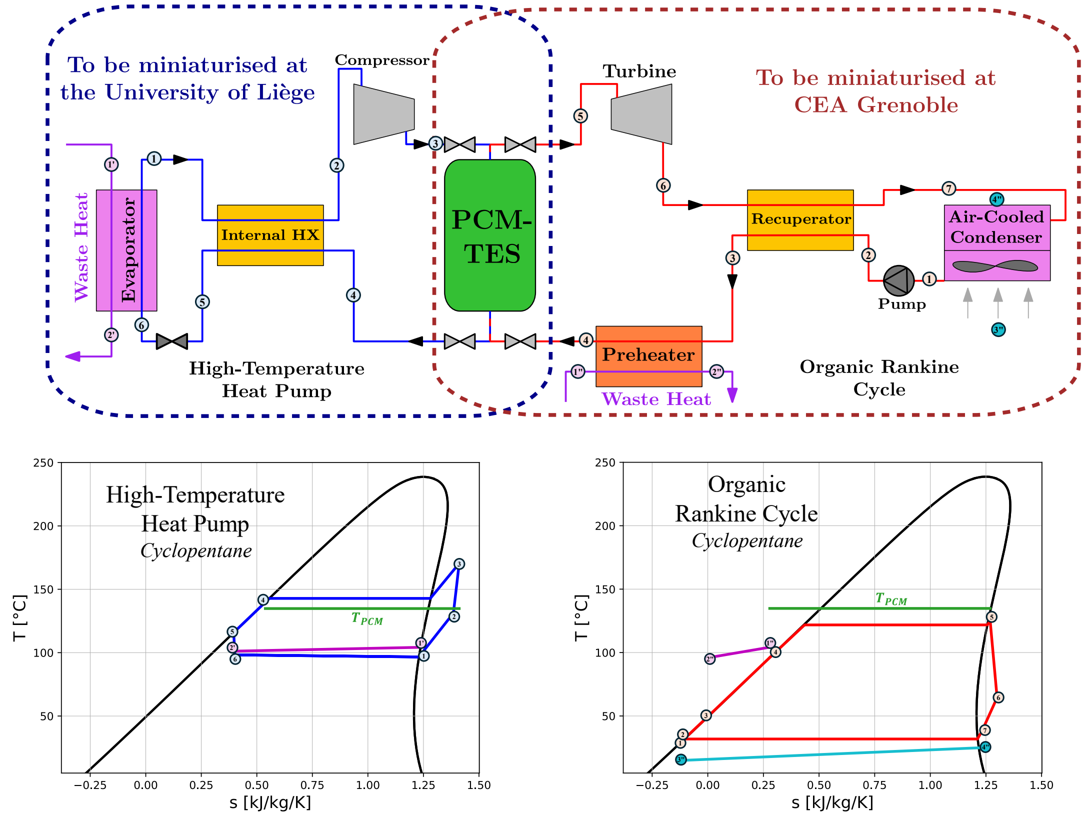

Figure 1: Architecture and T-s diagrams of the Zorlu Enerji use case of the SEHRENE project and relation with the TRL4 prototype to be built at the University of Liège and at CEA Grenoble.

2.2. *Test rig size and temperature level selection*

This section aims to describe the different choices made on test rig design, according to the heating capacity of the HTHP, and according to its temperature levels, mainly in terms of maximum condensation or heat sink temperature.

The base of the design starts with the TES. This component features a metallic lattice structure cast around 16 Heat Transfer Fluid (HTF) tubes. PCM is immersed inside the shell of the TES, all around the lattice structure and the tubes.

The standard version of this TES to be used in the test rig was presented as a Proof Of Concept (POC) by Yvernault et al. in [9]. It demonstrated thermal powers comprised between 3 kW and 5 kW during charge for near-plateau behaviour. In this POC, the PCM was Crodatherm 74, melting at 74°C. The TES characteristics and experimental results obtained in [9] were presented in Table 2. As the HTF temperature supplied at the inlet of the TES was 85°C, the temperature glide applied between the HTF TES inlet and the PCM melting temperature was 11 K ($T_{in,TES} - T_{PCM}$). In the test rig, a comparable temperature glide of 15 K will be applied, to be justified later in this section. Since this glide will be bigger, the thermal power of the TES is expected to be higher than the one measured in [9]. For that reason, the heating capacity required by the HTHP was considered as being about 7 kW.

Table 2: characteristics of the TES and experimental results obtained in the POC presented by [9].

	TES characteristics				Experimental results in [9]		
Parameter	Lattice structure type	Dimensions	Porosity	N° of HTF tubes	T_{PCM}	ΔT_{glide}	$\dot{Q}_{TES}$
Unit		[m]	[-]		[°C]	[K]	[kW]
Value	Kelvin open-cells	1×0.5×0.5	85%	16	74	11	3-5

To mimic the Zorlu Enerji use case of the SEHRENE project, the HTHP test rig should aim to achieve similar temperature levels. The first guess to select the required temperature level from the HTHP was considered as being the condensing temperature of the working fluid at 15 K more than the PCM melting temperature ($T_{PCM} = 134.8$°C). If sebatic acid was used in the TES of the test rig, the required condensing temperature of the HTHP would be ~150°C.

After reaching manufacturers, none of them were able to offer any off-the-shelf compressor capable of reaching such condensing temperatures while having a heating capacity of around 7 kW as required. In the literature, experimental HTHPs were usually studied in machines having at least two times the required capacity, for data points corresponding to the required heat sink temperature ([10], [11], [12]).

Out of many other examples of experimentally tested HTHPs, a test rig developed at the Eastern Switzerland University of Applied Sciences comprising a compressor from *Bitzer* showed heating capacities close to the ones required for the HTHP to be built [13]. It achieved 6 to 10 kW of heating capacity with heat sink temperatures going up to 150°C ([14], [15]). Despite the ability of the test rig to reach such high sink temperatures, the authors highlighted the importance of not operating the test bench at too high temperatures for too long because the compressor's motor has a shut-off temperature of 110°C. As the HTHP role will be to charge the TES, the compressor shall be able to run during a few hours (~2 to 4 hours if compared to [9]). Running at too high temperatures would lead to motor shut-off, hence it was decided to fix the design condensing temperature of the HTHP to 130 - 135°C. The compressor planned for the HTHP is almost the same as the one used in the test rig discussed above, but it uses the high-temperature variant of the model (*Bitzer* 2DES in [13] vs 2DES<u>H</u>).

In the meantime, the *Tecumseh* compressor manufacturer showed an interest in leading experimental campaigns to try to reach high temperatures with one of their off-the-shelf compressor. In this frame, a compressor from their company will be also included in the test rig for specific test at high temperature, with a particular interest in the study of the compressor cooling strategies. However, the latter will not be used for coupling with the TES, it will be the role of the *Bitzer* compressor.

As the chosen *Bitzer* compressor appeared to be the available component with the lowest heating capacity (7 kW to 9 kW at the required T_{sink}), the TES thermal power is therefore constrained to remain close to this value. Looking back at the TES PoC from Yvernault et al. [9], the TES thermal power seems to be calculated from the HTF temperature difference. As the HTF exits the TES with a temperature close to T_{PCM} in near-plateau behaviour, demonstrating 3 kW to 5 kW of thermal power, the same behaviour is expected in the ULiège test rig. This now justifies the choice of 15 K for the imposed TES glide ($T_{in,TES} - T_{PCM}$), versus the 11 K implemented in the PoC.

From the selected temperature of the HTHP, the PCM to fill the TES was chosen in collaboration with partners from the SEHRENE project. Three PCMs were pre-selected for having melting temperatures in the previously defined criteria, corresponding to the HTHP condensing temperature (130-135°C) minus 15 K, i.e. between 115 and 120°C. These three pre-selected PCMs were magnesium chloride hexahydrate, A118 and erythritol. First corrosion tests led by the University of Leicester showed that erythritol was the least affected by corrosion PCM when exposed to stainless steel and aluminium alloys for one week at high temperature (130°C). Hence, erythritol was selected as the PCM to fill the TES of the test rig. Its melting temperature is 117°C [16].

2.3. Working fluid choice

To address the WF choice to be used in the core loop of the HTHP, first the HFC are eliminated for the pre-selection as they have high Global Warming Potential (GWP) and are subject to phased-down measures under both the Kigali amendment of the Montreal protocol [17] and the EU F-gas regulation [18]. The facilities at the University of Liège does not include an ATEX zone, thus inflammable WF such as HCs were not pre-selected, even though they can show good performance [19]. The remaining candidates are HFOs and HCFOs. As the HTHP will require condensing temperature of about 135°C, WFs with too low critical temperatures were not pre-selected (R1234yf, R1234ze(E), R1336mzz(E)). Characteristics of the pre-selected WF were provided in Table 3.

Table 3: Characteristics of the pre-selected Working Fluids for usage in the test rig.

Fluid	GWP_{100}	ODP	TFA molecular yield	p_{crit}	T_{crit}	Normal boiling point	Safety class (ASHRAE)	Atmospheric lifetime	max $\dot{Q}_{HTHP}$ in [14]
			[-]	[barA]	[°C]	[°C]		[days]	[kW]
R1233zd(E)	1	0.00030 [20]	2% [20]	35.7	165.6	18.0	A1	46, 30.5, 40.4 [21], 26, 36 [20]	10.3
R1336mmz(Z)	7	0	20%	29.0	171.3	33.4	A1	105	7.7
R1224yd(Z)	0.88 [22]	0.00023 [22]	100% [23]	33.4	155.5	14.6	A1	20 [22]	10.0

The three pre-selected WFs were R1233zd(E), R1336mmz(Z) and R1224yd(Z). They were compared depending on their respective environmental impacts, and on their performance when used in the test bench developed at the Eastern Switzerland University of Applied Sciences [14], which comprised the same compressor than the one to be included in the test rig.

As the will of the test rig is to use the HTHP to charge the TES by melting its PCM, its limiting element shall not be the HTHP. Hence, the HTHP shall be able to always provide a sufficient thermal power to the TES. In [14], utilisation of R1336mmz(Z) showed maximum heating capacities of 7.7 kW, 46 to 76% lower than the one of R1233zd(E) depending on the data point. This was justified by the lower Volumetric Heat Capacity (VHC) of the R1336mmz(Z) compared to other fluids. In the meantime, selecting this fluid will mean buying bigger components, leading to a more expensive test rig, and in the end a more expensive product if willing to push it for commercial use. For these reasons, R1336mmz(Z) was not selected.

R1224yd(Z) showed heating capacities 9% higher than the ones of R1233zd(E) in average in the experimental campaign of Eastern Switzerland University of Applied Sciences. However, both WFs were able to reach sufficient heating capacity compared to what will be needed for charging the TES, with 10.0 and 10.3 kW for R1224yd(Z) and R1233zd(E), respectively. The main concern to be highlighted about the usage of the R1224yd(Z) is its environmental impact. Although its GWP and ODP are low, R1224yd(Z) shows a molecular potential for degradation to Trifluoroacetic Acid (TFA) estimated at 100% by [23]. TFA is an acid belonging to the family of per- and polyfluoroalkyl substances (PFAS) which is highly soluble in water, stable in the environment and thus prone to accumulate in terminal sinks [24]. This high solubility makes it difficult and energy costly to eliminate from water. TFA reported liver toxicity and disruptive effects on reproduction for mammalians [25]. Arp et al. highlighted the importance of reducing TFA emissions as current research does not place yet any clear threshold on TFA concentration that will have irreversible effects on local and global scale, and as some effects might be undiscovered yet [26]. They also proposed to classify this substance as a potential planetary boundary threat. Moreover, the European REACH regulation currently under consultation might forbid the usage of R1224yd(Z) [27]. For all these reasons, R1224yd(Z) was not selected as the WF to be used in the test rig.

Finally, R1233zd(E) seems to be a good trade-off as it combines sufficient heating capacity with the compressor to be used and low environmental impact (~2% of TFA molecular yield [20]). It will be the WF used in the test rig.

As the initial goal of the test rig was to mimic one of the use case of the SEHRENE project, it is relevant to justify why the chosen WF are not the same for both applications. First, cyclopentane (use case WF) is an inflammable refrigerant and thus cannot be used in ULiège facilities (no ATEX zone). Then, R1233zd(E) yields lower round-trip efficiency when assessed in the SEHRENE use case preliminary design.

3. Modelling the prototype for main components choice

This section aims to present the architecture of the test rig and the thermodynamic model developed to assess the design conditions of the test rig for components choice.

3.1. Test rig architecture

The test rig architecture is presented through its simplified P&ID on Figure 2.

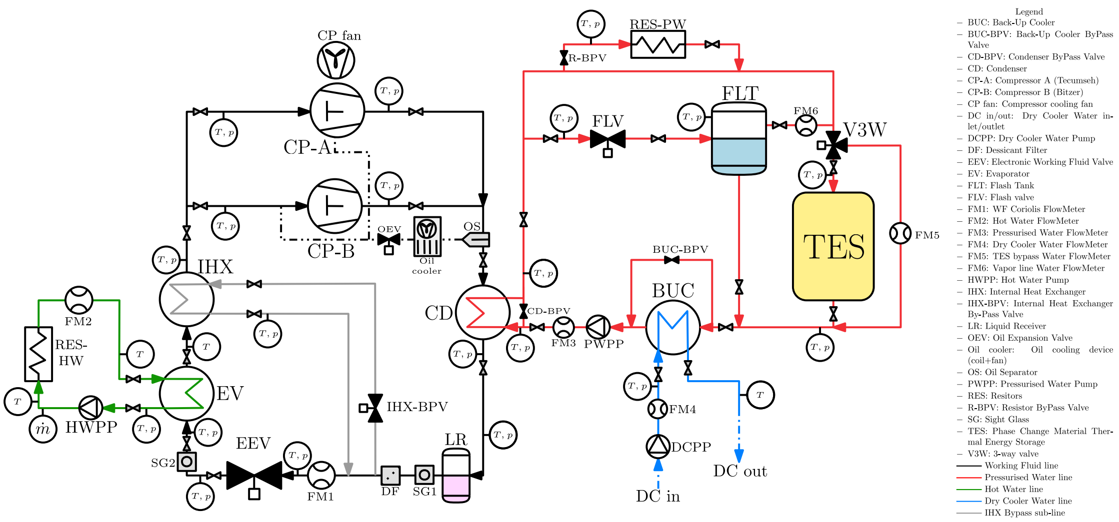

Figure 2: simplified P&ID of the test rig.

The main HTHP is composed of an evaporator, a condenser, an IHX, two compressors and an expansion valve. The expansion valve will be of the electric type to allow control in the WF loop. The evaporator, condenser and IHX will be plate heat exchangers (HXs). The mass flow rate fraction passing through the IHX will be controlled from 0 to 100% by a bypass valve. The two compressors are placed in parallel and are not meant to be used at the same time. Their role are distinct:

- Compressor A, supplied by *Tecumseh*, will allow the realisation of some tests on compressor cooling to push the compressor to high temperatures.
- Compressor B (*Bitzer*) will be used when coupling the HTHP to the TES for TES charging, named "HTHP+TES" configuration.

When the HTHP is not coupled with the TES (possible with both compressors), the configuration is referred to as "HTHP-alone". An oil separator is placed downstream the two compressors. The oil will be cooled, expanded and supplied back to the shell of the compressor (for CP-A, *Tecumseh*) through a dedicated port or to the suction of the compressor (for CP-B, *Bitzer*). A fan can also be used to cool any compressor by forced convection. For compressor A (hermetic), airflow is directed towards the shell, as some internal components must remain below their allowable temperature. For compressor B (semi-hermetic), the fan primarily cools the electric motor as it also needs to remain below a maximum temperature (110°C). Intermediate vapor injection of WF is not available on the selected compressors.

To supply heat to the HTHP mimicking an IWH source, a closed loop circulates water from resistors to the evaporator of the HTHP. The maximum hot water temperature is 110°C. A pump circulates the water in its loop.

At 135°C, the WF is expected to have a pressure of 20.9 barA. Unfortunately, due to manufacturing limitations, the tubes inside the TES cannot withstand a pressure higher than 7 barA. This means that the WF cannot circulate directly inside the TES HTF tubes. For that reason, a secondary loop is implemented in the test rig (red loop in Figure 2). This loop is used both in HTHP+TES and HTHP-alone configurations. In HTHP+TES configuration, its role is to transfer the heat from the HTHP condenser to the TES. The fluid circulating in this loop is Pressurised Water (PW). The condenser of the HTHP heats up this pressurised water which can deliver it to the TES in two forms: liquid or two-phase. In liquid mode, the liquid PW acts like a simple HTF and deliver its heat to the TES without phase changing. In two-phase mode, the PW is expanded in a valve to flash the water. The flash tank collects the two-phase water at the flash valve exhaust and allow the separation by gravity of the saturated vapor and the saturated liquid. The saturated vapor then goes to the TES to transfer to it some of the thermal power from the HTHP's condenser. In the meantime, the saturated liquid flows directly to the process point at the TES exhaust. The reason for the implementation of that flashing feature is that it will allow the studying of a two-phase flow inside the pipes of the TES while keeping the pressure below the manufacturing constrains. This two-phase flow condition might allow better heat transfer between the PW and the TES compared to simple liquid PW.

A Back-Up Cooler (BUC) is placed downstream the TES exhaust, also corresponding to the saturated liquid side of the flash tank exhaust if in two-phase mode. It exchanges heat between the PW loop and a tertiary loop of a dry cooler already existing in the lab. The BUC is materialised by a plate HX and fulfils four distinct roles:

- In HTHP-alone configuration, the thermal power from the condenser is transferred to the BUC by bypassing the flashing devices (top line, red loop) and the TES (rightmost line, red loop). The BUC then evacuates the heat to the tertiary dry cooler loop. The use of this intermediate heat sink loop rather than directly cooling the condenser with any cooling water (tap, dry cooler, etc.) is common in the literature ([13], [28], [29]).
- When the pressurised water loop is running in two-phase mode, the mixing of the water at the TES exhaust and the saturated water at the flash tank exhaust might lead to thermodynamic water state near saturation. The BUC allow the pressurised water to be fully condensed and sufficiently subcooled before entering the pump. This way, the constrains on the pump's required NPSH will be lowered. Furthermore, a physical NPSH will also be implemented.
- In liquid or in two-phase mode (HTHP configuration), the thermal power that the TES will be able to withstand will depend on its State of Charge (SoC). At high SoC, the TES will be able to exchange less thermal power than at the beginning of its charge. Hence, the remaining thermal power will be evacuated in the BUC.
- Finally, the BUC allows a quite simple discharge of the TES by circulating the pressurised water only in the TES and in the BUC while cooling the latter. The advantage of this feature is that there is no need of placing piping in the TES specifically for discharge, as it would have been the case if TES pipes were meant to contain direct WF.

A separated heating resistance will be placed in the liquid line of the PW loop to allow TES charging independently from the HTHP. The bypass regulation of the TES will be operated by a three-way valve. Manual valves will be placed at the extremities of each main components to allow the separation of each component from the circuit if some specific maintenance is needed. Thermocouples and pressure sensors will be placed at the most important locations of the test bench. The mass flow rate of the main HTHP loop will be measured thanks to a Coriolis flowmeter which will be situated after the liquid receiver and the IHX to ensure that it only contains subcooled liquid WF. Water flowmeters will be placed in the resistor, PW and mains water loops. Pumps will ensure the circulation of water in their respective loops.

3.2. Test rig modelling

To allow a good selection of components to be included in the test rig, it is crucial to perform an overall design of the test bench. This subsection describes the inputs, parameters and hypotheses considered for test rig dimensioning.

3.2.1. Compressor semi-empirical fitting

As the compressor represents the core element of the HTHP, its modelling needs to be as precise as possible. In this test rig, the two compressors to be included in the test bench were simulated using two different semi-empirical models.

The compressor A (from *Tecumseh*) is a hermetic piston compressor and was modelled according to the semi-empirical model of Brahami et al. [30]. The compressor was divided into multiple heat exchanging control volumes: suction line/upper cavity, oil/lower cavity, discharge line, mechanical kit and motor. 16 parameters are needed for compressor fitting. Data from a manufacturer internal experimental campaign were provided to find the parameters of the model corresponding to the compressor. As no test were carried out yet with the WF to be used in the test rig (R1233zd(E)), parameters were fitted to data from a different fluid (R455A). However, the semi-empirical model used is dimensionless so it allows extrapolation to different refrigerants. The parameters were fitted according to the refrigerant mass flow rate ($\dot{m}_{wf}$), compressor's exhaust temperature ($T_{ex,cp}$), compressor top shell temperature ($T_{top,cp}$) and compressor's oil temperature ($T_{oil,cp}$). Parity plots resulting from the parameters fitting were presented on Figure 3.

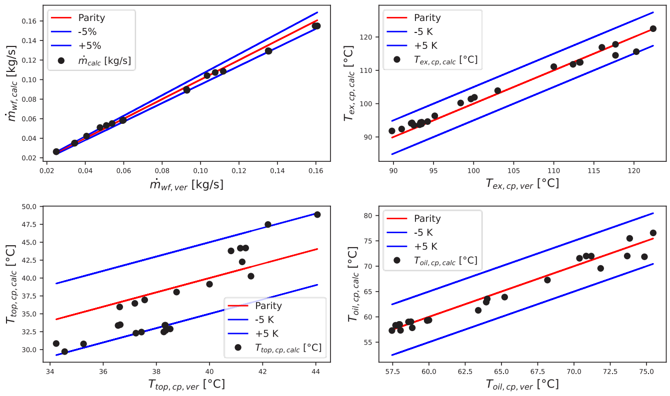

Figure 3: Parity plots representing the comparison between manufacturer experimental data and modelled data for the compressor A.

The compressor B is a semi-hermetic compressor from *Bitzer* and was selected in section 2.2. It was modelled according to the semi-empirical model of Winandy et al. [31] from data found on the Bitzer software website [32]. Here again, no data points were available for R1233zd(E), so R1234ze(E) was used for fitting. The latter was the available WF of the software comprising the highest critical temperature. Also, although the available data originated from a prior modelling effort rather than experimental measurements, they still offered a workable foundation for calibrating the semi-empirical model.

After finding the parameters corresponding to each of the compressors, the semi-empirical models were included in the test bench general design model.

3.2.2. Test rig overall modelling

Two distinct thermodynamic models were developed on the EES software [33], comprising the semi-empirical models corresponding to the compressor A and B, respectively. For each of the overall models, the following assumptions were made:

- Steady-state operation.
- WF expansion valve considered isenthalpic.
- Neglecting heat losses to the surroundings for all the test rig elements except the compressor (HXs, piping, expansion valve). The compressor exchange with the ambient is considered in each of the semi-empirical sub-models.

The phase-changing heat exchangers (evaporator & condenser) were modelled thanks to an imposed pinch point by their discretisation into two or three zone depending on WF phase, according to [34]. To ensure a conservative design, pinch points of 2 K and 3 K were selected for the condenser and evaporator, respectively. The condenser features a smaller pinch point because, unlike the evaporator where the working fluid flows against gravity, its flow direction is assisted by gravity [35]. Superheating and subcooling of 1 K were considered since the useful latter's are drastically increased thanks to the IHX. The latter was modelled with a constant effectiveness of 0.8. In the evaporator, the glide imposed for secondary fluid (hot water) was fixed at 3 K. This was the glide applied by Arpagaus at al. in [36] and this choice appeared relevant because the small glide allowed the hot water to exhibit large velocities, hence allowing it to stay turbulent in the evaporator, ensuring proper heat transfer in the latter.

For choosing the HTHP+TES configuration design point, the test rig was assumed to be running for thermal stabilisation before switching the TES into the circuit. In this mode, the HTHP provides thermal power to the PW loop while the TES is bypassed. The BUC rejects all the thermal power produced by the HTHP. The PW is considered as staying liquid without being flashed. This allows the pre-dimensioning of the BUC. To prepare the charging of the TES, the test rig must impose at BUC boundaries similar conditions than the ones to be seen when using the TES. The TES glide ($T_{in,TES} - T_{PCM}$) of 15 K, justified at section 2.2, is applied to choose the BUC inlet temperature. A glide of 5 K is imposed in the BUC. This results in BUC inlet and outlet temperatures of 132°C and 127°C, respectively.

As the test rig aims to be the miniaturisation of a SEHRENE TI-CB, the design point was set by reproducing the temperature lift ($T_{sat,cd} - T_{sat,ev}$) of the HTHP in the Zorlu Enerji use case preliminary design, corresponding to 45.4 K. In the EES model, this parameter is fixed by definition of the evaporating temperature as an input.

Dry cooler water flows in the BUC of the test rig with a considered inlet temperature of 10°C. The input to play with to design the BUC is the outlet temperature. Modelling the latter with a constant rather good effectiveness ($\varepsilon = 0.8$) was leading to an outlet temperature above 100°C, not possible in real conditions since water needs to return to the dry cooler loop in liquid form. To obtain a conservative pre-design of the BUC, i.e. to somehow maximise its area, this HX needs to see a minimised Log Mean Temperature Difference ($LMTD = (\Delta T_{hot} - \Delta T_{cold})/\ln(\Delta T_{hot}/\Delta T_{cold})$). This LMTD is minimised when the mains water outlet temperature is maximised, so the latter value was set to 95°C.

The parameters, inputs, and results of the modelling were reported in Table 4.

Table 4: Parameters, inputs and results of the overall test rig modelling for component selection.

	Parameters							Inputs				Pre-design results		
Parameter	ε_{IHX}	ΔT_{sc} ΔT_{sh}	ΔT_{ev}^{glide}	ΔT_{ev}^{pp}	ΔT_{cd}^{pp}	ΔT_{BUC}^{glide} ΔT_{cd}^{glide}	T_{PCM}	$T_{su,DC}$	$T_{ex,DC}$	$T_{sat,ev}$/ ΔT_{lift}	f_{cp}	$\dot{Q}_{ev}$	$\dot{Q}_{cd}$	$\dot{Q}_{BUC}$
Unit	[-]	[K]	[K]	[K]	[K]	[K]	[°C]	[°C]	[°C]	[°C]	[Hz]	[kW]	[kW]	[kW]
Value	0.8	1	3	3	2	5	117	10	95	88.6/ 45.4	50	13.3	16.5	16.5

Thermodynamic models for both HTHP-alone et HTHP+TES modes were compared. The results showed larger thermal powers in HTHP+TES configuration, hence, the design point was chosen as being the one for that mode.

Although the current study presents only one design point, the selection of the suitable components for the test rig is undertaken by modifying the latter on occasion. For the HXs, the most conservative design point was the one for which the required HXs heat duties were maximal. This conservative design point can be different for other types of components. Moreover, full operating ranges (minimum to maximum values) are sent to component suppliers and subsequently verified. All this procedure will allow the proper running of the test rig even in off-design operation.

Components manufacturers started to be contacted at the time of the paper redaction.

4. Learning potential outcomes

This section aims to describe how the test rig will allow potential learning outcomes, that both might be able to be applied to small-scale implementations and large-scale theoretical systems studied in the SEHRENE's project use cases.

First, in HTHP-alone configuration, the test rig will try to push forward the boundaries of the existing compressor A in terms of maximum temperature, even if the latter was not designed for that. This will particularly allow the exploration and comparison of different cooling methods of the compressor: blowing air on its shell, cooling the oil from the oil separator and reinjecting it on a dedicated port or at the compressor suction. Moreover, the test rig will allow the characterisation of the compressor using R1233zd(E), which was not performed yet by the manufacturer.

The test rig in HTHP-alone configuration will also be operated with compressor B. It will notably be the case when testing the loop with the flashing features and TES bypassed, to perform a commissioning campaign allowing a progressive increase in experimental tests complexity. Both "HTHP-alone" experimental campaigns will aim to push small HTHP technologies to higher TRL, as they could find market applications in food, paper, metal or chemical industries [5].

The test rig in HTHP+TES configuration will allow to assess multiple technical questions. First, the dynamic behaviour of the system will be studied. The dynamic behaviour of the TES alone could be analysed if proper thermal conditioning of the TES is made prior to its charging. Also, the dynamics of all the elements of the HTHP+TES combined together will be able to be investigated. This could give some insights to determine the start-up time of the system. The experimental results will be compared with a numerical model to be developed. This latter point might allow the results to be upscaled to the machines modelled is the SEHRENE project's use cases.

In HTHP+TES configuration and flashing water mode, the whole test rig will see four phase changes at the same time: WF evaporating in the evaporator, WF condensing in the condenser, PW being flashed then condensed in the TES tubes, and PCM being melted in the TES shell. This rather complex configuration will certainly require the placement of control devices at strategic locations of the test rig. The components able to be controlled will be:

- The resistors thermal power and target temperature, i.e. the evaporator thermal power.
- The hot water loop pump (green on Figure 2), i.e. the hot water mass flow rate.
- The compressor speed, from an external inverter.
- The electronic expansion valve of the WF in the main HTHP loop.
- The IHX bypass valve, for useful superheating control.
- The PW pump, for PW mass flow rate control.
- The flashing valve pressure drop.
- The 3-way-valve used for TES bypassing.
- The dry cooler water pump, i.e. the cooling water flow rate.

As multiple components will be controllable, different methods could be implemented and compared to find the best control strategy. To some extent, the resulting optimal control strategy might be applied to the large-scale theoretical systems studied in the SEHRENE project's use cases.

An initial hypothesis was that the TES charge as described in [9] exhibited near-plateau behaviour. Actually, at the beginning of the thermal charge, the TES displays thermal powers up to 35 kW ; 15 kW after 5.8 min ; 10 kW after 16.7 min. Controlling the HTHP so that it can provide a thermal power at each point equivalent to the one required by the TES seems overly ambitious. Hence, the first control strategy to be implemented on the test rig will be the bypass of the TES. This will keep its required thermal power nearly-constant, thereby enabling the HTHP to operate in a near-steady-state regime, far easier to control.

Despite the PW loop being an added feature resulting from a manufacturer constraints ($p_{max}^{TES} < p_{required}$), the loss of performance due to the addition of an intermediate loop could be compensated for by the higher heat transfer coefficients of water (in both condensing and liquid regimes) compared with organic fluids [37]. Furthermore, the experimental campaign will also compare TES performance when using the flashing device in the PW loop to operation with PW staying in liquid phase (e.g. on $\dot{Q}_{TES,max}$).

5. Conclusion

In conclusion, this paper describes the prototyping of a test rig to be constructed at the University of Liège. This test rig aims to be the downscale of the charging phase of the TI-CB concept promoted in the EU-funded SEHRENE project, consisting of a HTHP charging a PCM-based TES. The HTHP heating capacity and temperature level are designed to fulfil the charge of the TES depending on compressor availability in the market and from a literature review. The chosen compressor will allow the HTHP to run with a condensing temperature of 135°C at 10 kW of thermal power. Erythritol is selected as the Phase Change Material to fill the TES (melting temperature of 117°C). Another compressor will also be included in the test rig to conduct specific tests on it cooling.

Test rig features are presented: the two compressors to be included in the test rig will not have the same purpose. One will be used for specific tests on its cooling, the other for usage in the full HTHP coupled with TES. Because of TES manufacturing constraints, a secondary PW loop is included between the HTHP and the TES. This loop allows TES charging from PW either being in liquid phase or in two-phase thanks to a flashing device composed of a flash valve and a flash tank. A Back-Up Cooler is added in the PW loop to be used when TES bypassing, TES nearly fully charged, TES discharge and for proper subcooling of the water before the water pump (NPSH). R1233zd(E) is identified as the best working fluid for this application, after comparisons of several candidates in terms of performance and environmental impact. The authors want to highlight the importance of considering the working fluids TFA molecular yield when designing thermodynamic systems as the choices of today might have an important impact on public health for current and future generations.

The design point for components choices is elaborated from thermodynamic models comprising semi-empirical sub-models of the two compressors to be included in the test rig. From the models outputs, a design point is presented for components selection. The test rig will allow testing in single HTHP configuration to study compressor cooling. When coupled with the PW loop, i.e. with the TES, the test rig will allow the testing and comparison of several control strategies with results hopefully to be upscaled to larger TI-CB applications. Finally, the relevance of the flashing device in the PW loop will be assessed.

Acknowledgements

The project that produced the results presented in this paper has received funding from the European Union's Horizon Research and Innovation programme under grant agreement No. 101135763, in the framework of the SEHRENE project. The authors thanks Dr. Yacine Brahami from Tecumseh Europe for the technical support on the feasibility of the test rig and providing compressors.

References

[1] O. Dumont, G. F. Frate, A. Pillai, S. Lecompte, M. De paepe, and V. Lemort, ‘Carnot battery technology: A state-of-the-art review’, *Journal of Energy Storage*, vol. 32, p. 101756, Dec. 2020, doi: 10.1016/j.est.2020.101756.
[2] ‘SEHRENE: Store Electricity and Heat foR climatE Neutral Europe’, Sehrene Project. Accessed: Nov. 10, 2025. [Online]. Available: https://sehrene.eu/
[3] M. Peeters, E. Neven, O. Dumont, and V. Lemort, ‘Preliminary experimental investigation of a 10 kWe thermally integrated pumped thermal energy storage system using a reversible organic Rankine cycle/heat pump’, in Proceedings of the 8th International Seminar on ORC Power Systems. Sep. 2025.
[4] A. Cendoya, F. Ransy, B. Guo, A. Hernandez, O. Dumont, and V. Lemort, ‘Design and modelling of a reversible HP/ORC Carnot battery tailored for waste heat integration in flooded mines’, *Applied Energy*, vol. 404, p. 127127, Feb. 2026, doi: 10.1016/j.apenergy.2025.127127.
[5] C. Arpagaus, F. Bless, M. Uhlmann, J. Schiffmann, and S. S. Bertsch, ‘High temperature heat pumps: Market overview, state of the art, research status, refrigerants, and application potentials’, *Energy*, vol. 152, pp. 985–1010, Jun. 2018, doi: 10.1016/j.energy.2018.03.166.
[6] A. Cendoya, B. Chaudoir, T. Janod, T. Hazar, U. Halaçoğlu, and V. Lemort, ‘Carnot Battery Integration in a Geothermal Power Plant: Study Case of Zorlu Enerji’, in Proceedings of Carnot 2024 : Belgian Symposium of Thermodynamics. 2024. doi: 10.5281/zenodo.17964654.
[7] D. Alfani *et al.*, ‘Integration of an Electro-Thermal Energy Storage (ETES) System in a Geothermal Power Plant’, in Proceedings of the European Geothermal Congress 2025.
[8] M. Carlo d’Incalci, D. Alfani, and P. Bombarda, *Preliminary Analysis of an Electro-Thermal Energy Storage System for Geothermal Applications*. in Proceedings of the 8th International Seminar on ORC Power Systems. Lappeenranta-Lahti University of Technology LUT, 2025. Accessed: Oct. 06, 2025. [Online]. Available: https://lutpub.lut.fi/handle/10024/170511
[9] L. Yvernault, S. Vesin, and J. Pouvreau, ‘Experimental characterisation and numerical modelling of a novel heat exchanger for latent heat thermal energy storage composed with open-cells metallic lattice structure cast around tubes’, *Journal of Energy Storage*, vol. 152, p. 120714, Mar. 2026, doi: 10.1016/j.est.2026.120714.
[10] N. Deng *et al.*, ‘Molecular simulation and experimental investigation for thermodynamic properties of new refrigerant NBY-1 for high temperature heat pump’, *Energy Conversion and Management*, vol. 179, pp. 339–348, Jan. 2019, doi: 10.1016/j.enconman.2018.10.076.
[11] C. Mateu-Royo, J. Navarro-Esbrí, A. Mota-Babiloni, F. Molés, and M. Amat-Albuixech, ‘Experimental exergy and energy analysis of a novel high-temperature heat pump with scroll compressor for waste heat recovery’, *Applied Energy*, vol. 253, p. 113504, Nov. 2019, doi: 10.1016/j.apenergy.2019.113504.
[12] M. Ramirez, F. Trebilcock-Kelly, J. L. Corrales-Ciganda, J. Payá, and A. H. Hassan, ‘Experimental and numerical investigation of a novel high-temperature heat pump for sensible and latent heat delivery’, *Applied Thermal Engineering*, vol. 247, p. 122961, Jun. 2024, doi: 10.1016/j.applthermaleng.2024.122961.
[13] C. Arpagaus, F. Bless, M. Uhlmann, E. Büchel, and S. Frei, ‘High temperature heat pump using HFO and HCFO refrigerants - System design, simulation, and first experimental results’, 2018.
[14] C. Arpagaus and S. Bertsch, ‘Experimental Comparison of HCFO and HFO R1224yd(Z), R1233zd(E), R1336mzz(Z), and HFC R245fa in a High Temperature Heat Pump up to 150 °C Supply Temperature’, 2021.
[15] L. P. M. Brendel, C. Arpagaus, J. Pfaffl, F. Simon, and S. S. Bertsch, ‘Disassembly of Off the Shelve Reciprocating Compressor After Employment in High-Temperature Heat Pump for More Than 1000 Operating Hours’, 2024.
[16] J. Pereira Da Cunha and P. Eames, ‘Thermal energy storage for low and medium temperature applications

using phase change materials – A review', *Applied Energy*, vol. 177, pp. 227–238, Sep. 2016, doi: 10.1016/j.apenergy.2016.05.097.
[17] E. A. Heath, 'Amendment to the Montreal Protocol on Substances that Deplete the Ozone Layer (Kigali Amendment)', *International Legal Materials*, vol. 56, no. 1, pp. 193–205, Feb. 2017, doi: 10.1017/ilm.2016.2.
[18] *Regulation (EU) 2024/573 of the European Parliament and of the Council of 7 February 2024 on fluorinated greenhouse gases, amending Directive (EU) 2019/1937 and repealing Regulation (EU) No 517/2014*. 2024. [Online]. Available: http://data.europa.eu/eli/reg/2024/573/oj
[19] O. Bamigbetan, T. M. Eikevik, P. Nekså, M. Bantle, C. Schlemminger, and M. Dallai, 'Experimental Investigation of a Hydrocarbon Piston Compressor for High Temperature Heat Pumps', *International Compressor Engineering Conference*, Jan. 2018, [Online]. Available: https://docs.lib.purdue.edu/icec/2634
[20] M. P. Sulbaek Andersen, J. A. Schmidt, A. Volkova, and D. J. Wuebbles, 'A three-dimensional model of the atmospheric chemistry of *E* and *Z*-CF3CH=CHCl (HCFO-1233(zd) (E/Z))', *Atmospheric Environment*, vol. 179, pp. 250–259, Apr. 2018, doi: 10.1016/j.atmosenv.2018.02.018.
[21] M. K. Vollmer, S. Reimann, M. Hill, and D. Brunner, 'First Observations of the Fourth Generation Synthetic Halocarbons HFC-1234yf, HFC-1234ze(E), and HCFC-1233zd(E) in the Atmosphere', *Environ. Sci. Technol.*, vol. 49, no. 5, pp. 2703–2708, Mar. 2015, doi: 10.1021/es505123x.
[22] K. Tokuhashi, T. Uchimaru, K. Takizawa, and S. Kondo, 'Rate Constants for the Reactions of OH Radical with the (*E*)/(*Z*) Isomers of CF_3 CF═CHCl and CHF_2 CF═CHCl', *J. Phys. Chem. A*, vol. 122, no. 12, pp. 3120–3127, Mar. 2018, doi: 10.1021/acs.jpca.7b11923.
[23] D. D. Behringer *et al.*, 'Persistent degradation products of halogenated refrigerants and blowing agents in the environment: type, environmental concentrations, and fate with particular regard to new halogenated substitutes with low global warming potential'.
[24] K. R. Solomon *et al.*, 'Sources, fates, toxicity, and risks of trifluoroacetic acid and its salts: Relevance to substances regulated under the Montreal and Kyoto Protocols', *J Toxicol Environ Health B Crit Rev*, vol. 19, no. 7, pp. 289–304, 2016, doi: 10.1080/10937404.2016.1175981.
[25] W. Dekant and R. Dekant, 'Mammalian toxicity of trifluoroacetate and assessment of human health risks due to environmental exposures', *Arch Toxicol*, vol. 97, no. 4, pp. 1069–1077, Apr. 2023, doi: 10.1007/s00204-023-03454-y.
[26] H. P. H. Arp, A. Gredelj, J. Glüge, M. Scheringer, and I. T. Cousins, 'The Global Threat from the Irreversible Accumulation of Trifluoroacetic Acid (TFA)', *Environ. Sci. Technol.*, vol. 58, no. 45, pp. 19925–19935, Nov. 2024, doi: 10.1021/acs.est.4c06189.
[27] 'Per- and polyfluoroalkyl substances (PFAS) - ECHA'. Accessed: Nov. 13, 2025. [Online]. Available: https://echa.europa.eu/hot-topics/perfluoroalkyl-chemicals-pfas
[28] F. Kaufmann, J. von Zabienski, L. von Ribbeck, M. Ehmann, H. Spliethoff, and C. Schifflechner, 'Experimental analysis of a reversible high-temperature heat pump/ORC test rig for geothermal CHP applications', *Applied Thermal Engineering*, vol. 280, p. 128360, Dec. 2025, doi: 10.1016/j.applthermaleng.2025.128360.
[29] J. Jeßberger, F. Heberle, and D. Brüggemann, 'Experimental optimization of the part load behaviour of a high-temperature heat pump', in Proceedings of the 8th International Seminar on ORC Power Systems. Sep. 2025.
[30] Y. Brahami, M. Metral, and D. Leray, 'A dimensionless hermetic reciprocating compressor thermal model', in press. 2026.
[31] E. Winandy, C. Saavedra O, and J. Lebrun, 'Simplified modelling of an open-type reciprocating compressor', *International Journal of Thermal Sciences*, vol. 41, no. 2, pp. 183–192, Feb. 2002, doi: 10.1016/S1290-0729(01)01296-0.
[32] 'BITZER SOFTWARE'. Accessed: Nov. 12, 2025. [Online]. Available: https://www.bitzer.de/websoftware/
[33] F-Chart Software., 'Engineering Equation Solver (EES) Manual'. Accessed: Jan. 31, 2025. [Online]. Available: https://www.fchart.com/assets/downloads/ees_manual.pdf
[34] C. Cuevas, J. Lebrun, V. Lemort, and P. Ngendakumana, 'Development and validation of a condenser three zones model', *Applied Thermal Engineering*, vol. 29, no. 17, pp. 3542–3551, Dec. 2009, doi: 10.1016/j.applthermaleng.2009.06.007.
[35] S. Kloczko and A. Faghri, 'Thermal performance and flow characteristics of two-phase loop thermosyphons', *Numerical Heat Transfer, Part A: Applications*, vol. 77, no. 7, pp. 683–701, Apr. 2020, doi: 10.1080/10407782.2020.1714342.
[36] C. Arpagaus and S. S. Bertsch, 'Experimental results of HFO/HCFO refrigerants in a laboratory scale HTHP with up to 150 °C supply temperature', in Book of presentations of the 2nd Symposium on High-Temperature Heat Pumps. SINTEF, 2019.
[37] S. Kakaç, H. Liu, and A. Pramuanjaroenkij, *Heat Exchangers*, 0 edn. CRC Press, 2012. doi: 10.1201/b11784.